Polaron Transport Mechanism in Maricite $NaFePO_4$: A Combined Experimental and Simulation Study

Monika Sharma[1], Sevi Murugavel[1], and Payam Kaghazchi[2]

[1]Department of Physics and Astrophysics, University of Delhi, Delhi–110 007, India
[2]Forschungszentrum Jülich GmbH, Institute of Energy and Climate Research, Materials Synthesis and Processing (IEK-1), Wilhelm-Johnen-Straße, 52425 Jülich, Germany

We report, for the first time, systematic investigations on electronic properties of maricite $NaFePO_4$ with different crystallite sizes by a combined experimental and theoretical approach. Ac impedance spectroscopy has been used to study the polaron transport behavior in maricite $NaFePO_4$ structure with different crystallite sizes over a wide range of temperatures. With the decrease in crystallite size, we observe a polaronic conductivity enhancement of approximately an order of magnitude at the nanoscale level as compared with its bulk counterpart. The temperature dependent dc conductivity has been analysed within the framework of the Mott model of polaron hopping and various physical parameters relevant for the polaron hopping process were extracted. Additionally, by introducing an approximated Mott model with calculated hole polaron migration barrier from density functional theory, we evaluated the polaronic conductivity as function of crystallite size in fair agreement with experimental data. The enhanced polaronic conductivity with crystallite size reduction is found to be due to the combined effect of increased polaron concentration, reduced hopping length, and lowered migration barrier.

I. INTRODUCTION

Lithium based rechargeable batteries have been considered as an attractive power source for a wide variety of applications, such as portable electronic devices and electric vehicles. The material research has been dedicated for discovering the new electrode material as well as an improvement in the existing cathode materials to make the superior performance characteristics of the lithium ion batteries (LIB). The main concern in the development of cheaper, safe and high-power cathode material is to replace the conventional $LiCoO_2$ due to its high price, toxicity and possesses problematic safety features. In this context, during last two decades potentially important cathode materials such as $LiNiO_2$, $LiMn_2O_4$, and olivine compounds have been considered as possible cathode material for LIB[1-4]. More specifically, olivine compounds $LiMPO_4$ (M= Mn, Fe and Ni) have attracted much attention than other class of cathode materials by the battery community because of their three-dimensional framework structure stabilized by strong covalent bonds between the oxygen and phosphorus tetrahedral polyanions[5, 6].

Within the olivine phosphate structures, $LiFePO_4$ (LFP) has been ruling the world of cathode materials for the large-scale applications of the LIB with its unique features like flat charge-discharge voltage profile, environment safely, and low-cost[7, 8]. In spite of its many advantages, the performance of LFP has been hindered by its poor electronic and ionic diffusivity resulting into the sluggish electrochemical performance. In order to improve the electron diffusivity, various approaches have been developed including doping with aliovalent cation, carbon coating, mesoporous structure and reduced particle sizes[9-12]. Despite of all the efforts taken in improving the performance, the high cost and limited resources of lithium-based electrode material, now the interest has been renewed in the favour of sodium ion batteries (SIB) over the LIB. Sodium is available majorly in the earth's crust and oceans, however, being heavier in size more precisely three times weightier as compared to the lithium,

the mobility of Na^{+} becomes smaller. Despite the disadvantage in terms of its size, sodium ion batteries find its applications in the large-scale applications such as electric grid applications. In the recent years considerable amount of research has been dedicated in developing the LFP equivalent of cathode materials for the sodium ion batteries (NIBs).

Different research groups have reported the electrochemical properties of the $NaMO_2$ (M=Fe and Co), which is analogue to currently used commercial cathode materials for rechargeable batteries[13]. In this regard, Nazar et al. and many other research groups[14-16] showed the possibility of redox reaction with the conversion of Fe^{2+} to Fe^{3+} in the polyanionic compounds like Na_2FePO_4F and $Na_2FeP_2O_7$. Additionally, the covalent bonding of the P-O network provides structural stability but it reduces the theoretical capacity as well. Herein, we explore Na analogue of LFP with theoretical capacity exceeds all the above mentioned Fe base electrode materials such as Na_2FePO_4F (120 $mAhg^{-1}$), $Na_2FeP_2O_7$ (90 $mAhg^{-1}$), and $Na_4Fe_3(PO_4)_2(P_2O_7)$ (130 $mAhg^{-1}$) for sodium ion batteries leading to 155 $mAhg^{-1}$ and with Coulombic efficiency of 92% [15, 17-19]. The Na analogue of LFP, $NaFePO_4$ (NFP) exists in two different phases, namely, the olivine and maricite structure. The thermodynamically stable phase of NFP is the maricite phase and it can be synthesized by the conventional chemical routes, whereas the unstable olivine NFP structure can only be produced by the electrochemical route[17, 20]. The difference between the two phases arises in terms of their structure where the site occupancies of metal ions differ. In the case of olivine phase, the M1 sites are occupied by the Na^{+}, while M2 sites occupied with Fe^{2+}. On the other hand, in maricite phase situation become opposite, where Fe^{2+}occupies the M1 sites, while Na^{+} occupies the M2 sites. Since the distance between M2 sites in maricite is larger, it has been assumed that the hopping of Na^{+} becomes energetically less favourable. In olivine structure, Na^{+} involving octahedra share edges in the structure and form zig-zag chains along the *b*-direction in the structure which is the favourable direction for Li ion hopping in the structure. The previous reports on olivine

structured LFP revealed that the transport of the lithium or sodium ion takes place 1D channel conduction along *b*-direction.[21, 22] On the other hand, due to site interchange of metal ions in maricite structure, the free 1D channel conduction becomes impossible and hence reduced Na^+ transport leads to electrochemically inactivity in maicite structure based cathode material[23, 24].

The recent study on the m-NFP structure reveals the possibility of the two-dimensional Na^+ transport in the structure with reduced the particle size[25]. According to this study, at lower particle sizes (<50 nm), the transport of Na^+ is feasible in the *bc* plane along with the structural change. However, the enhanced cycling performance (after the first cycle) of the active cathode material has been ascribed to the amorphous structure, where diffusion length of Na^+ becomes smaller in comparison with pristine structure. In addition to marcite structured Na based cathode material, olivine type $NaFePO_4$ has been investigated by using theoretical approach such as density functional theory (DFT) and compared with olivine $LiFePO_4$ system[26]. These studies revealed that the migration energy of sodium in olivine structured NFP is 0.05 eV higher than that of lithium ion in olivine LFP. Islam and his co-workers[27] have used DFT method to compare the sodium ion conduction process in olivine $NaMPO_4$ (Fe, Mn) with the layer-structured Na_2FePO_4F. Notably, the DFT study reveals that the migration energy barrier for Na^+ conduction in olivine $NaFePO_4$ along the 1D channel is slightly lower than for lithium ion migration in $LiFePO_4$.

More commonly, the electron transport in transition metal oxide systems takes place via the hopping of the small polarons, which is hole polaron in the present case. The important quantities for deciding the performance of cathode materials are the kinetics involving the electronic and ionic diffusion. Hence, it is important to understand the electron diffusion in m-NFP structure. Up to date, to our knowledge, there is no experimental report on the polaronic conduction in m-NFP structure. Therefore, we have carried out detailed experimental

investigations on m-NFP structure by understanding the polaron transport mechanism as well as to improve their mobility by reducing the particle/crystallite size.

Density functional theory (DFT) calculation is a powerful tool to study migration mechanism of electron/hole polarons in cathodes. Zhou et al. pointed out that it is important to include the Hubbard term (U) into DFT-PBE and -LDA calculation to account for the electron/hole localization in LFP.[28] Mechanisms of polaron migration in olivine structured LFP and $LiMnPO_4$ as well as olivine-NFP (O-NFP) have been then investigated using DFT-PBE+U.[29, 30] We have also recently computed polaron formation in Maricite NFP[31] and polaron migration in $LiCoO_2$[32] using DFT-PBE+U calculation.

In this direction, we have undertaken systematic investigations on m-NFP by combining experimental and theoretical methods. A single phase m-NFP has been obtained by the solid state route with different crystallite sizes starting from bulk (80 nm) to 25 nm. With the help of various analytical techniques, we have confirmed all the samples crystallize in *maricite* structure without any parasitic phase's contributions. Broadband impedance spectroscopy has been used to study the polaron transport in all the crystallite sizes with different temperatures. With the reduction of crystallite size, we find polaronic conductivity enhancement of approximately an order of magnitude at the nanoscale level as compared with its bulk counterpart. Additionally, the electronic properties and polaronic conductivity of m-NFP with different sodium vacancy concentration have been studied by using DFT-PBE+U and the Mott theory of polaron conduction. The results obtained from theoretical study complement with the experimental data and unpin the underlying mechanism for the enhanced polaronic conductivity. The enhanced polaronic conductivity at lower crystallite size could open door for the electrochemically inactive bulk m-NFP as promising cathode material for advanced sodium batteries.

II. METHODOLOGY

A. Experiment

Stoichiometric m-NFP with different crystallite sizes has been prepared by using the solid-state route. The precursors used for the synthesis were of high purity Na_2CO_3, $FeC_2O_4.2H_2O$ and $NH_4H_2PO_4$ in stoichiometric ratio mixed together and grinded to homogenize the mixture. Afterwards, the mixture was then transferred to the alumina boat and fired at 750°C in the reducing atmosphere, which results the bulk sample with the 80 nm crystallite size. In order to synthesize the lower crystallite sized particles, we have varied the synthesis temperature along with the process timings and the relevant synthesis parameters can found elsewhere[31]. Further, we have characterized all our m-NFP samples by x-ray diffraction (XRD), x-ray absorption spectroscopy (XAS), Field Emission Scanning Electron Microscopy (FESEM) and High resolution transmission electron microscopy (HRTEM) and the results have been reported in our earlier work[31]. An obtained powdered sample was grinded and moulded into various shapes for further characterizations. Subsequently, we have analysed the phase formation and absence of any parasitic phases by the angle dispersive x-ray diffraction measurements. Based on the obtained XRD data, we have estimated the crystallite size by separating the contribution of strains dominating at nano scale-level with the help of Williamson Hall relation[33].

Ac impedance spectra of different crystallite sizes were made on the circular disc (pellet) shaped samples with 13 mm diameter and 1mm thickness by using the α-S High resolution dielectric analyser. The required amount of m-NFP powder was first pressed into pellet by using stainless steel die and by means of uniaxial press (4 Ton). Ionically, blocking electrodes were made by sputtering silver/gold layers on both sides of the compact disc to have Ohmic contacts. The ac impedance measurement was performed over a frequency range of 10

mHz to 1 MHz, at temperatures between 253 K and 573 K. The dc conductivity has been extracted by fitting the frequency-dependent conductivity spectra by using the Jonscher power law relation. Additionally, the optical band gap has been measured using the UV-Vis spectroscopy with diffuse reflectance mode. In diffuse reflectance mode, the absorption spectra of the samples have been recorded using the suspension made with ethanol over the range of 200 to 1100 nm. The reference spectrum was recorded using the pure ethanol without any sample followed by the mixture consists of sample and ethanol. The Tauc plot has been derived from the diffuse reflectance data, and then, the optical band gap of respective crystallite size was estimated.

B. Computation

Spin polarized DFT calculations were carried out using the projector-augmented plane-wave (PAW) method as implemented in the Vienna Ab Initio Simulation Package (VASP)[34]. The crystal lattice parameters and density of states (DOS) have been computed using the Perdew-Burke–Ernzerhof (PBE) functional[35] as well as PBE with Hubbard *U* parameter (U_{eff} =*U*-*J*)[36]. The *U* value was chosen such that i) our experimental band gap value for the pristine m-NFP was reproduced and ii) a hole was trapped on Fe site. The wave function has been expanded by using a plane wave basis set with an energy cut-off of 520 eV for all the calculations.

The atomic structures and spin density differences (SDDs) were visualized by the software VESTA[37]. The primitive unit cell of m-NFP possess a orthorhombic structure with P*mnb* space group containing four formula units with 4 Na, 4 Fe, 4 P, and 16 oxygen atoms. In our recent work,[31] we have modelled different concentrations of the following defects in NFP: (1) hole-polaron on Fe cations (2) neutral Na vacancy, i.e. Na_+ vacancy + hole-polaron on Fe cations, and (3) Na+ vacancy. It was found that the lattice parameters changes are mainly driven

by hole-polaron formation. Hence, to calculate the crystallite-size-dependent polaronic conductivity, we modelled various crystallite sizes with supercells having a similar percentage of polaronic centres to our experimental results as listed in Table 1. For example, based on experimental results, the 25 nm crystallite-size system shows a polaronic concentration of 14 %. For our calculations, we modelled a system with a polaronic concentration of 12.5 % to examine the behaviour of 25 nm crystallite size. Please note that the supercell sizes have been chosen in such a way to have one hole-polaron per unit cell. This is because within the DFT calculation we have no direct control over the local position of electron density which makes it difficult to trap two or more separated polarons in a supercell. Moreover, calculation of migration pathway for one polaron out of two or more polarons in a unit cell is even technically more problematic. This is because during the migration of a polaron, the formation of other trapped polarons might get affected or even we might get delocalized holes distributed over all Fe sites rather than localized polarons.

The optimized lattice parameters and the corresponding applied Monkhorst–Pack *k*-point meshes with the chosen *U* parameter of 5.0 eV are also listed in Table 1. Formation of hole polaron was achieved by the removal of an electron from a Fe^{2+} site. To localize the hole polaron at a Fe site, the bond lengths of the FeO_6 octahedra were changed slightly such that the equatorial Fe-O bonds became longer and axial Fe-O bonds became shorter. The migration of hole polaron from one site to the another was investigated by finding the minimum energy path (MEP) using the nudged elastic band (NEB) method considering nine replicas of the structure between the initial and final positions. Furthermore, using the migration energy barrier as well as the defect concentration (i.e. hole-polaron concentration) in each structure, the polaronic conductivity has been calculated for various crystallite sizes using an approximated Mott theory polaronic conduction. We also studied the effect of changing the *U* value on the polaronic conductivity for m-NFP with 75 nm crystallite size. The increase of *U* value enhances

the hole localization on Fe sites leading to the increase in hopping distance and migration barrier, and thereby it will lead to the reduction in electronic conductivity. For example, the polaronic conductivity for the 75 nm crystallite size with 2% sodium vacancies in the structure decreases by one order of magnitude with increasing the *U* value from 5.0 to 8.0 in the calculations.

III. Results and Discussion

A. ac impedance measurements

The ac impedance of all the m-NFP samples with different crystallite sizes have been carried out using broadband dielectric analyser with wide range of temperatures. The frequency dependent conductivity spectra of bulk m-NFP (80 nm) sample measured at different temperatures is shown in figure. 1. The electrical conductivity measurements were limited to lower temperatures up to 253 K due to the very high impedance of the sample. The real part of the measured ac conductivity can be considered as the sum of two components i.e. frequency dependent part and frequency independent part which is typical characteristics of polaron conducting glasses and crystal[38, 39]. At high temperatures and sufficiently low frequencies, the measured conductivity is found to be independent of frequency, which corresponds to thermally activated dc conductivity. On the other hand, at high frequencies and lower temperatures in addition to dc conductivity the measured conductivity includes the frequency dependent, where hopping of polarons takes place among the nearest neighbouring sites via correlated forward-backward hopping motions.

In general, the low-frequency dc conductivity and high-frequency ac conductivity regions are separated by a characteristic frequency, (ν^*), defined arbitrarily by $\sigma'(\nu^*) = 2\sigma_{dc}$. Similarly, we have observed temperature and frequency dependent ac conductivity behaviour for all the crystallite sizes of m-NFP. The real part of ac conductivity has been analysed by using various approaches in the literature including different class of materials, which provide

important information about the nature of charge transport at various length scales[40, 41]. The typical dc conductivity value from each isotherm for given crystallite size was extracted from the measured frequency dependent conductivity spectra by using the Jonscher's power law relation[42] and is given by:

$$\sigma(\upsilon) = \sigma_{dc}\left[1 + \left(\frac{\upsilon}{\upsilon^*}\right)^s\right] \qquad (1)$$

where σ_{dc} is the dc conductivity for a particular temperature, ν^* is the characteristic or crossover frequency where the behaviour of conduction changes (from long-range to short-range hopping) and s is the Jonscher's exponent whose value lies in the range $0 < s \leq 1$ related to the dimensionality of the charge transport of given system[43]. For most of the ion and polaron conducting glasses and crystals, the exponent value (s) tends to increase with decreasing the temperature and approaches unity at sufficiently low temperatures. Furthermore, we have extracted the dc conductivity by fitting the frequency dependent conductivity spectra with the help of equation 1. The apparent dc conductivity is exclusively attributed to the contribution of intrinsic bulk part and neglect grain boundary contributions. The variation of dc conductivity for different crystallite sizes at 313 K is illustrated in figure 2. Until now there is no report on the polaronic conductivity measurement on the m-NFP either in bulk form or nano sized crystallites. With the continuous decrease in crystallite size down to 25 nm, we observe the increase in the polaronic conductivity of m-NFP.

UV Visible spectroscopy of all crystallite sizes were recorded in reflectance mode over a wide wavenumber range. The m-NFP is an indirect band gap semiconductor and the band gap has been estimated by using the Tauc relation[44]. The crystallite size dependent behaviour of polaronic conductivity is substantiated by the changes in the corresponding optical band gap and is depicted in figure 2. It can be seen very clearly that the variation of polaronic

conductivity and optical band gap value complements each other with the decrease in the crystallite size. As confirmed by the XRD along with vibrational spectroscopy measurements where there is no other contribution of parasitic phases for the measured conductivity values, which confirms obtained conductivity values are intrinsic part of m-NFP structure. It is interesting to note that the decrease in the crystallite size leads to the enhancement in the dc conductivity significantly whereas the reverse trend is seen for the optical band gap values. An increment in the dc conductivity with nanosizing can be understood further with the help of the various physical parameters related to polarons which are estimated within the framework of Mott model of the small polaron hopping.

In figure 3(a), we present the obtained dc conductivity in the Arrhenius plot for all the crystallite sizes of m-NFP sample measured over a wide range of temperatures. It is clear from the figure 3a that the measured dc conductivity data do not follow the simple Arrhenius behaviour instead we find two different temperature regions corresponding to intermediate or quasi-adiabatic regime and high-temperature or non-adiabatic regime with a positive slope as shown in figure 3b. We define that the crossover from the intermediate (I_t) to high-temperature (H_t) is equal to half the Debye temperature (θ_D) and is given by:

$$h\upsilon_{ph} = k\theta_D \qquad (2)$$

where υ_{ph} is the longitudinal optical (LO) phonon frequency. The obtained Debye temperature for all the crystallite sizes is listed in Table 2. It is clear that the estimated Debye temperature for bulk m-NFP sample is close to the value reported for O-LFP sample[12]. It is interesting to note that the decrease in θ_D with crystallite size indicates the reduction in the total vibrational energy spectrum in m-NFP. In general, the θ_D is a characteristic nature of solid lattice linked to its phonon spectrum, where it represents nearly all the modes of vibration is excited at a specific temperature[45].

It is known that in transition metal oxides (TMOs), electrical conduction mechanism is mainly governed by phonon assisted polaron hopping between the localized sites[45]. In general, the obtained dc conductivity for the nearest-neighbour hopping in the non-adiabatic region is given by:

$$\sigma_{dc} = \upsilon_p \left[\frac{e^2 c(1-c)}{k_B T R} \right] \cdot \exp(-2\alpha R) \exp\left(-\frac{E_a}{k_B T} \right) \quad (3)$$

where, ν_p is the longitudinal optical phonon frequency, R is the distance between two neighbouring Fe ions, α is the inverse localization length of s-like wave function, c is the ratio of the concentration of polaronic sites (Fe^{3+}) over the total amount of Fe ions in the matrix and this value is directly related to the concentration of sodium ion vacancies[46]. The dc conductivity at each temperature has been extracted by using the Jonscher's relation (Eq.1). The temperature dependent dc conductivity has been analysed by using the Eq. (3) and extracted the various physical quantities involved in hopping transport of polarons are listed in Table. 2. In TMO's, the small polarons are highly localized and it is characterized by the inverse localization length of 1.5-2 $Å^{-1}$. In this work, the rate of wave function decay or inverse of localization length has been found to be 1.2-1.5 $Å^{-1}$ and similar values have been reported on the different TMO's .

In m-NFP, it could be considered that polaron hopping takes place along the *b* direction since the FeO_6 octahedra is edge-shared along this direction and the hopping distance of the interlayer (5.163 Å) is larger than the intra chain (3.4009 Å) hopping distance. The hopping of polarons along the interlayer would cost higher activation energy because the edge-shared FeO_6-FeO_6 units are tied by the neighbouring PO_4 units in corner-sharing fashion. Thus, the inter site distance along the chain (*b-direction*) corresponds to the typical polaron hopping length, i.e. distance between the two neighbouring Fe sites. Remarkably, we find from the present analysis of equation (3), the hopping length of small hole polaron is 3.453 Å for bulk m-NFP, which is close the two neighbouring Fe sites. We have also obtained the hopping

distance for polaron between the two iron sites from our theoretical studies on the m-NFP structure which will be discussed in the next section. Again, the reduction in hopping length of m-NFP with the crystallite size can be attributed to the change in Fe-O bond length, which ultimately leads to 2 % contraction in the unit cell volume at the nano scale level.

For the case of olivine structure the most common defects are the alkali ion vacancy and the anti-site defects[47, 48]. In the case of anti-site defect structure, the alkali ion and the transition metal ion reverse their position each other. In olivine structure, the formation of anti-site defects hinders the motion of alkali ion thereby reducing the Na_+ diffusivity in the structure. The formation energy for the anti-site defects in the olivine phase of LFP and NFP has been studied with the application of strain and found that anti-site defect formation energy is lower for the Na analogue of the structure[49]. The formation energy of the anti-site defect pair in O-NFP is almost 0.42 eV which is much lower than the O-LFP having 0.7 eV and it makes the diffusion of Na difficult in the structure. On the other hand, there are no reports on the structural defects in the m-NFP structure. Additionally, it is important to mention that we don't find significant amount of anti-site defect sites in the structure with the Rietveld refinement procedure even for the lowest crystallite size 25 nm in the present work.

We have fitted the experimental dc conductivity data with Mott model shown in figure 3b and extracted the various polaron hopping parameters listed in Table 2. Clearly, with the reduction in the crystallite size the different hopping parameters shows the substantial variation with crystallite size (listed in the table 2). The major contribution for the increase in dc conductivity results from the reduction in activation energy, hopping length and an increase in the polaron concentration. Firstly, the migration barrier for the polaron hopping (one Fe site to the nearby site) decreases with decrease in the crystallite size, which is beneficial for the total dc polaronic conductivity. Another important quantity is the polaron concentration which increases again with decrease in the crystallite size due to the surface energy kinetics as well

as relatively low formation energy of sodium ion vacancy[50]. Interestingly, the obtained polaron concentration with crystallite size from Mott equation shows the significant dependency. In the present case, the creation of a sodium ion vacancy leads to the hole polaron, i.e. the oxidation of transition metal changes along with the local distortion in the structure (here $Fe^{2+} \rightarrow Fe^{3+}$). Thus, each sodium ion vacancy act as source for the polaron formation and due to surface energy kinetics its concentration increases with decrease in the crystallite size. Correspondingly, we also determined the sodium ion vacancy concentration from Rietveld refinement analysis, where it increases systematically with decrease in the crystallite size and complement with each other. For the case of transition metal oxide based systems, the mobile charge carriers are the polarons which can be localized electron or hole depending on the valance state of metal ion. The lithium addition or withdrawal during the charging and discharging of the battery the conduction takes place via the electron or hole polaron in the electrode material respectively. With the creation of the hole polaron in the structure the oxidation of transition metal changes along with the local distortion in the structure.

The decrement in the hopping length with the reduction in the crystallite size is also favoured for the polaron conductivity enhancement at lower crystallite size. In compensation with the contraction of hopping parameter R, the inverse localization length α increases. Using α and R, we have estimated exp(-2αR) for different crystallite sizes (see Table 3). Both the parameters vary in such a way to make the overall variation in the tunnelling probability negligible. An estimated hopping length for the bulk m-NFP is found to be around 3.453 Å and it decreases continuously to a value of 2.947 Å for the 25 nm crystallite size. Hence, the observed enhanced polaronic conductivity at lower crystallite size is attributed to the combined effect of polaron concentration, hopping length, and reduced activation energy.

B. Electronic structure of pristine m-NFP

In figure 4, we depict the calculated density of states (DOS) for pristine m-NFP with DFT-PBE and DFT-PBE+U. The m-NFP material is known as the indirect band semiconductor and its computed band gap using PBE+*U*=5 eV agrees better with the experimental value in comparison to those calculated using PBE and PBE+*U* with other *U* values (cal.: 2.4 eV and exp.: 2.36 eV). Thus, the particular *U* value of 5 eV was used for the rest of our calculations. In other olivine structures such as LFP, different values of *U* (3.5 eV) have been used in literature[27], while Shuye et al. have used U value of 4.3 and 4.5 eV for LMP (M= Mn and Fe)[51]. Because of the relatively large band gap of m-NFP, the electron-hole transport in this material proceeds via small-hole-polaron hopping. The optimization of electronic structure reveals that m-NFP is a weak ferromagnetic system with a magnetic moment of 3.90 μ_B per Fe atom which is close to earlier reports in the literature[52]. A recent study has reported that the rutile-LFP possesses chains of trans-edge sharing FeO_6 octahedron are ferromagnetically ordered within the chain and with the moments localized on the *ac* plane[53]. They further found that the chains are linked anti-ferromagnetically, although the quasi one-dimensional character of the magnetic structure and the arrangement of the chains are in a closely ideal triangular pattern. In iron oxides with the valance state of Fe^{2+}, the electronic states at the top of the valence band and bottom of the conduction band should be predominantly d-states of the metal. In the m-NFP structure, Fe exist in high spin with the $[t_{2g}]^4[e_g]^2$ configuration of the five electrons in the spin up state where as the remaining one electron sits in the t_{2g} state with spin down configuration. The valance band maximum (VBM) is mainly contributed by the t_{2g} spin down polarized electron as can be seen in calculated DOS in figure 5.

C. Hole polaron formation

The hole-polaron formation takes place at the Fe^{2+} site resulting in a localized gap state close to VBM (figure 6). Our calculations show analogous gap-state formation to figure 6 for

higher concentrations of hole-polaron in the smaller crystallite sizes than 75 nm. It has already been suggested by Maxisch *et al*. that the hole polaron formation in olivine-LMP (M: transition metals) structures arises from the Fe *3d* states and not from the oxygen 2p states on the top of the valance band[29]. If Fe-3d states dominates the VBM, small hole polaron can form and there will be a redox centre, whereas if the oxygen character dominates the VBM, the hole created at the expanse of electron withdrawal will be delocalized. Moreover, Johannes et al. found that the hole polaron formation in Fe-based olivine-LMP structure costs less energy than the counterpart Ni- and Mn-based structure[54].

It is important to mention that our DFT calculations show that the m-NFP structure with a localized hole-polaron has a lower energy in comparison to that with a delocalized hole distribution. The hole-polaron has a spin-down state after one Fe^{2+} site is converted into Fe^{3+} site (see Fig. 6). Similar gap sates with spin down character have also been observed in DOS plots of olivine (Li, Na) phosphates with hole-polarons[55]. The arrow marked in figure 7 shows the direction of the oxygen-anion displacement after formation of a hole-polaron.

A main parameter controlling the properties of small-crystallite size materials is the formation of defects, which, in the present case, are mainly Na vacancies together with hole-polarons on Fe sites (to preserve the charge neutrality of the system). Formation of defects can strongly affect electronic conductivity via change in the concentration and/or migration barrier of charge carriers, i.e. hole-polarons. The latter effect can be very strong as the energy barrier is in the exponent of the Arrhenius equation. It has been recently reported that the migration barrier of polarons varies with lattice parameters[26] that can change with concentration of Na vacancies, for example, with nanosizing[31] and/or sodiation/desodiation during charge/discharge[56] of cathodes. Our recent combined experimental (X-ray diffraction and X-ray absorption spectroscopy) and theoretical (DFT) study showed that the lattice parameters contraction induced by the decrease of crystallite size of m-NFP is driven by hole-polaron

formation in crystals that coexist with Na_+ vacancies (charge neutralization).[31] Other factors such as surfaces do not have significant contribution but it must be present at minimal level. Thus, in this work, we have used the optimized supercells listed in Tab. 2 for m-NFP with different hole-polaron concentrations to calculate the polaronic conductivity as function of crystallite size.

D. Hole polaron migration and polaronic conductivity

In our calculations, we trapped a polaron on different Fe sites and always found that localization of a polaron induces a lattice change mainly along the *b* direction. The local distortions and lattice parameter change for single polarons at different Fe sites are very similar (difference of < 0.01 Å). Hence, we have considered the polaron hopping from an arbitrary Fe site and only along the *b* direction to study the effect of concentration of defects on the conductivity. Moreover, the distance between Fe ions is smallest along the *b* direction (3.447 Å) as compared to the *a* and *c* direction, and therefore the electronic transport should occur mainly along the *b* direction.

To visualize the hole polaron migration in the structure we have calculated SDDs for initial, final, and transition states (see figure 7). For the case of transition state, the polaron is delocalized among two Fe sites labelled as Fe1 and Fe2, while in the initial and final structures the polaron is localized at Fe1 and Fe2, respectively. The migration energy barrier calculated for the m-NFP sample with the lowest studied concentration of polaron, namely 2%, is around 300 meV which is slightly higher than the previous theoretical results on olivine LFP with approximately 1% hole concentration[29,35]. The theoretical calculations by Kresse *et al.* show a lower activation energy and higher electronic conductivity value as compared to the experimental values reported by Murugavel *et al.* for LFP [12]. In the present case, we have observed a close agreement between the experimental and the calculated conductivity values

which will be discussed further. Our calculations indicate (see Table 4) that migration barrier decreases with polaron concentration. Afterwards, we have calculated the polaronic conductivity of the m-NFP with the help of estimated migration barrier and concentration of holes (considered to be the same as Na_+ vacancies based on the charge compensation mechanism of cathode materials). For the bulk sample with 80 nm crystallite size which reflects almost negligible vacancy concentration, the polaron localization and conductivity were not calculated due to the computational limitations. We have estimated the polaronic conductivity for different crystallite sizes (as listed in Table 1) by using the following relation:

$$\sigma = n_h e \mu_h = n_h e(1-c)\left(\frac{ega^2\vartheta_p}{k_B T}\right).\exp(-2\alpha R)\exp\left(\frac{-\Delta E}{k_B T}\right), \quad (4)$$

where n_h, e, g, a, v_p, k_B, and T are the concentration of hole polaron, charge state of an electron, geometric pre-factor, jump distance, characteristic phonon frequency, Boltzmann constant, and temperature, respectively. The concentration of hole polaron is expected to be equal to the concentration of Na vacancies in the structure (V_{-Na}). For example, the value of n_h for m-NFP with 75 nm crystallite size is evaluated to be 2.594x 10^{-4} $Å^3$ i.e. one hole per 3 × 2 × 2 supercell (theoretical unit-cell parameters of 15.312 Å×13.814 Å×18.188 Å). The value of $(ega^2v_p)/k_BT$ at T = 300 K for a wide range of materials is almost equal to 1 $cm^2/(V.s)$[57]. Thus, we approximated the value of $(ega^2v_p)/k_BT$ to be equal 1 $cm^2/(V.s)$ for the calculation of polaronic conductivity. The term exp(-2αR), which is the probability of tunnelling, includes two parameters, namely the inverse localization length (α) and hopping distance (R). From the experimental dc conductivity results, we have extracted the values of α and R using the Mott model. However, for our calculations, we estimated only R for different hole-polaron concentrations and found quite similar values to the experimental ones. To our knowledge, there is no well-defined approach to compute parameter α. This is because there is no clear definition of this parameter on the electronic scale. Nevertheless, the extracted value of the

whole term exp(-2αR) for all different crystalline sizes is about 1.03 (see Tab. 3). The values differ only at the third decimal place. For this reason and also in order to maintain the individuality of experimental and theoretical methods, we did not use the experimentally evaluated α values for DFT calculations. Instead, we considered the exp(-2αR) term to be about 1 for all the calculations. Our previous calculation on electronic conductivity of $LiCoO_2$ using the Nernst-Einstein theory was in good agreement with the experimental value.[32] The difference between our approximated Mott theory and Nernst-Einstein is only the presence of the (1-c) factor in the former one. The value of this factor for a low concentration of hole is close to 1, and therefore, our calculated σ for $Li_{0.96}CoO_2$ using the Nernst-Einstein theory was in fair agreement with the experimental σ.[32] However, for m-NFP with small crystallite sizes, i.e. high concentrations of hole-polarons, including the (1-c) factor to the Nernst-Einstein theory, i.e. approximated Mott theory, improved our predicted σ values.

The variation of calculated conductivity as function of polaronic concentration (figure 8) is very similar to the experimental values. The increase in dc conductivity with the decrease in the crystallite size is the consequence of the increase in the polaronic concentration as well as the decrease in the migration energy barrier. The latter is due to the contraction of lattice parameters with the increase in the hole-polaron concentration. The lowering of migration barrier is due to the increase in the overlap of *d* orbitals of Fe cations. Hence, we find a lower energy barrier for a smaller crystallite size. The jump distance in the bulk (ideal structure) m-NFP is shorter than that in the olivine LFP (3.78 Å)[12] leading to the higher polaronic conductivity of the former case.

IV. CONCLUSIONS

The detailed electronic properties of m-NFP with various crystallite sizes have been investigated by combining ac impedance spectroscopy, DFT calculations, and Mott theory. It is found that the dc polaronic conductivity of the m-NFP increases with the decrease in the

crystallite size. The enhancement in the dc polaronic conductivity at lower crystallite size has been attributed to the increase in the polaronic concentration, contraction of polaron hopping distance, and lowering of activation energy for polaron migration. The DFT study on the m-NFP reveals that the small hole polaron formation in the structure depends on the nature of VBM. The necessary condition for the hole polaron localization on the Fe centre is that the valance band maximum should be composed of metal 3d character. The polaronic conductivity calculated with our approximated Mott model with DFT-PBE+U data is in good agreement with our experimental results. Since doping of battery cathode materials with cations and/or anions can affect their lattice sizes,[58,59] our computational approach can, for example, be used in future to predict effect of doping on the electronic conductivity of cathode materials.

ACKNOWLEDGMENTS

The authors acknowledge the funding support from Erasmus Exchange Program. P. K. also acknowledges the Deutsche Forschungsgemeinschaft (DFG) under the grant number 383045781. M. S. and S. M. acknowledge the USIC, University of Delhi for providing the various characterizations facility during the course of work.

REFERENCES

1 M. Yonemura, A. Yamada, Y. Takei, N. Sonoyama and R. Kanno, J. Electrochem. Soc. **151**, A1352 (2004).

2 G. Chen, J. D. Wilcox, and T. J. Richardson, Electrochem. Solid-State Lett. **11(11)**, A190 (2008).

3 X. Xiong, D. Ding, Y. Bu, Z. Wang, B. Huang, H. Guoa and X. Lia, J. Mater. Chem. A **2**, 11691 (2014).

4 Y. Xia and M. Yoshio, J. Electrochem. Soc. **143**, 825 (1996).

[5] A. K. Padhi, K.S. Nanjundaswami and J. B. Goodenough, J. Electrochem. Soc. **144**, 1188 (1997).

[6] A. Yamada, Y. Kudo, and K. Y. Liu, J. Electrochem. Soc. **148**, A747 (2001).

[7] K. Zaghib, K. Striebel, A. Guerfi, J. Shim, M. Armand, and M Gauthier, Electrochimica Acta **50**, 263 (2004).

[8] L. H. Hu, F. Y. Wu, C. T. Lin, A. N. Khlobystov and L. J. Li, Nature Commun. **4**, 1687 (2013).

[9] S. Y. Chung, J. T. Bloking and Y. M. Chiang, Nat. Mater. **1**, 123,(2002).

[10] P. S. Herle, B. Ellis, N. Coombs and L. F. Nazar, Nat. Mater. **3**, 147 (2004).

[11] H. Huang, S. C. Yin and L. F. Nazar, Electrochem. Solid-State Lett. **4**, A170 (2001).

[12] R. Shahid, and S. Murugavel, Phys. Chem. Chem. Phys., **15**, 18809 (2013).

[13] A. Fouassier, G. Matejka, J. M. Reau, and P. Hagenmuller, J. Solid State Chem. **6** 532 (1973).

[14] B. L. Ellis, W. R. M. Makahnouk, Y. Makimura, K. Toghill and L. F. Nazar, Nat. Mater. **6**, 749 (2007).

[15] H. Kim, I. Park, D.H. Seo, S. Lee, S.W. Kim, W.J. Kwon, Y.U. Park, C.S. Kim, S. Jeon, K.Kang, J. Am. Chem. Soc. **134**, 10369 (2012).

[16] H. Kim, R. A. Shakoor, C. Park, S. Y. Lim, J. S. Kim, Y. N. Jo, W. Cho, K. Miyasaka, R. Kahraman, Y. Jung and J. W. Choi, Adv. Funct. Mater. **23**, 1147 (2013).

[17] M. Casas-Cabanas, V. V. Roddatis, D. Saurel, P. Kubiak, J. Carretero-Gonzalez, V. Palomares, P. Serras and T. Rojo, J. Mater. Chem. **22**, 17421 (2012).

[18] J. S. Ko, V. V. T. Doan-Nguyen, H.-S. Kim, X. Petrissans, R. H. DeBlock, C. S. Choi, J. W. Long and B. S. Dunn, J. Mater. Chem. A **5**, 18707 (2017).

[19] P. Barpanda, T. Ye, M. Avdeev, S.-C. Chung and A. Yamada, J. Mater. Chem. A **1**, 4194 (2013).

[20]N. V. Kosova, V. R. Podugolnikov, E.T. Devyatkina, and A.B. Slobodyuk, Material Research Bulletin **60**, 849 (2014).

[21]N. Nitta, F.Wu, J. T. Lee, and G. Yushin, Materials Today **18**, 252 (2015).

[22]M. S. Whittingham, Chem. Rev. **104**, 4271 (2004).

[23]A. Sun, F. R. Beck, D. Haynes, J. A. Poston, S. R. Narayanan, P. N. Kumta and A. Manivannan, Mater. Sci. Eng. B **177**, 1729 (2012).

[24]J. C. Lu, S. C. Chung, S. Nishimura and A. Yamada, Chem. Mater. **25**, 4557 (2013).

[25]J. Kim et al., Energy Environ. Sci. **8**, 540 (2015).

[26]M. Nakayama, S. Yamada, R. Jalem, and T. Kasuga, Solid State Ionics, **286**, 40 (2016).

[27]R. Tripathi, S. M. Sood, M. S. Islam and L. Nazar, Energy Environ. Sci., **6**, 2257 (2013).

[28]F. Zhou, C. A. Marianetti, M. Cococcioni, D. Morgan, and G. Ceder, Phys. Rev. B **69**, 201101 (2004).

[29]T. Maxisch, F. Zhou, and G. Ceder, Phys. Rev. B **73**, 104301 (2006).

[30]Y. Asari, Y. Suwa, and T. Hamada, Phys. Rev. B **84**, 134113 (2011).

[31]M. Sharma, M. Gupta, P. Kaghazchi, and S. Murugavel, Phys. Chem. Chem. Phys., **21**, 25206 (2019)

[32]A. Moradabadi and P. Kaghazchi, Phys. Rev. Appl. **7**, 064008 (2017).

[33]Y. Prabhu and K. V. Rao, World J. Nano Sci. Eng. **4**, 21 (2014).

[34]G. Kresse and J. Furthmuller, Phys. Rev. B **54**, 11169 (1996).

[35]J. P. Perdew, K. Burke, and M. Ernzerhof, Phys. Rev. Lett. **77**, 3865 (1996).

[36]S. L. Dudarev, G. A. Botton, S. Y. Savrasov, C. J. Humphreys, and A. P. Sutton, Phys. Rev. **B 57**, 1505 (1998).

[37]K. Momma and F. Izumi, J. Appl. Cryst. 41, 653 (2008).

[38]D. J. Huang, W. B. Wu, J. Okamoto, H.-J. Lin, and C. T. Chen, F. C. Chou, A. Fujimori, Phys. Rev. Lett. **94**, 146402 (2005).

[39]B. Roling and K. Funke, J. Non Cryst. Solids **212**, 1 (1997).

[40]D. L. Sidebottom, Rev. Mod. Phys. **81**, 999 (2009).

[41]J. C Dyre and T. B Schrøder, Rev. Mod. Phys. **72**, 873 (2000).

[42]A. K. Jonscher, Nature **267**, 673 (1977).

[43]D. L. Sidebottom, Phys. Rev. Lett. **83**, 983 (1999).

[44]J. Tauc, Mater. Res. Bull. **3**, 37 (1968).

[45]N. F. Mott, J. Non Cryst. Solids **1**, 1(1968).

[46]I. G. Austin and N. F. Mott, Adv. Phys. **50**, 757 (2001).

[47]M. Saiful Islam, D. J. Driscoll, C. A. J. Fisher, and P. R. Slater, Chem. Mater. **17**, 5085 (2005)

[48]G. K. P. Dathar, D. Sheppard, K. J. Stevenson, and G. Henkelman, Chem. Mater. **23**, 4032 (2011).

[49]L. Hong, L. Li, Y.-K Chen-Wiegart, J. Wang, K. Xiang, L. Gan, W. Li, F. Meng, F. Wang, J. Wang, Y.-M. Chiang, S. Jin and M. Tang, Nat. Commun. 8, 1194 (2017).

[50]M. M. Sundaram, T. Watcharatharapong, S. Chakraborty, R. Ahuja, S. Duraisamy, P. T. Rao, N. Munichandraiah, Dalton Trans. **44**, 20108 (2015).

[51]S. P. Ong, V. L. Chevrier, and G. Ceder, Phys. Rev. B **83**, 075112 (2011).

[52]M. Avdeev, Z. Mohamed, C.D. Ling, J. Lu, M. Tamaru, A. Yamada, P. Barpanda, Inorg. Chem. **52**, 8685 (2013).

[53]F. Zhou, M. Cococcioni, K. Kang, G. Ceder, Electrochem. Commun. **6**, 1144 (2004).

[54]K. Hoang, and M. Johannes, Chem. Mater. **23**, 3003 (2011).

[55]M. D. Johannes, K. Hoang, J. L. Allen, and K. Gaskell, Phys. Rev. B **85**, 115106 (2012).

[56] R. J. Clément1, P. G. Bruce, and C. P. Grey, J. Elec. Soc. **162**, A2589 (2015).

[57]A. J. E. Rettie, W. D. Chemelewski, D. Emin, and C. Buddie Mullins, J. Phys. Chem. Lett. **7**, 471 (2016).

[58]J. U. Choi, C. S. Yoon, Q. Zhang, P. Kaghazchi, Y. H. Jung, K-S Lee, D-C Ahn, Y-K Sun, and S-T Myung , J. Mater. Chem. A, **7**, 202 (2019)

[59]J. U. Choi, Y. J. Park, J. H. Jo, L-Y Kuo, P. Kaghazchi, and S-T Myung, ACS Appl. Mater. Interfaces, **10**(48), 40978 (2018)

Table 1. Lattice parameters as well as applied *k*-points for modelling various crystal sizes.

Supercell	**Super cell (unit cell parameters)**	**K POINTS**	**Na_+ vacancies (%) (expt. value)**	**Na atoms/ unit cell**	**Vacancies concentration (calculations)**	**Crystallite size (nm) (expt. value)**
3*3*2	15.312 Å x 20.721 Å x 18.188 Å	1x1x1	0.01	72	-	80

3*2*2	15.312 Å x 13.814 Å x 18.188 Å	3x3x3	1.75	48	2	75
3*2*1	15.312 Å x 13.814 Å x 9.094 Å	3x3x6	6	24	4.16	50
2*2*1	10.208 Å x 13.814 Å x 9.094 Å	3x3x6	9.5	16	6.25	40
1*2*1	5.104 Å x 13.814 Å x 9.094 Å	9x3x6	14.2	8	12.5	25

Table 2: Summary of important Mott parameters related to the polaronic dc conductivity for different crystallite sizes of m-NFP.

Crystallite Size (nm) ± 0.4 nm	**Debye Temp. (K)**	**ν_{ph} (10^{13} Hz)**	**R (Å) ± E_r**	**c (conc.)**	**Na_+ Vacancies (%)**	**E_a (H.T.) (eV)**	**E_a (I.T.) (eV)**
80	587.82	1.22	3.453 ±0.002	0.0001	0.01	0.395	0.32
75	580.74	1.20	3.447 ±0.001	0.0143	1.75	0.393	0.314
50	525.40	1.09	3.257 ±0.001	0.050	6	0.368	0.296
40	493.79	1.02	3.182 ±0.002	0.082	9.5	0.342	0.274
25	467.80	0.97	2.947 ±0.004	0.104	14.2	0.310	0.243

Table 3: Crystallite size dependent tunnelling parameter.

Crystallite size (nm)	**α (inverse location length) (cm^{-1})**	**R (hopping distance)(cm)**	**$e^{-2\alpha R}$**
75 nm	$1.2*10^6$	$3.447*10^{-8}$	1.035
40 nm	$1.27*10^6$	$3.182*10^{-8}$	1.034
25 nm	$1.385*10^6$	$2.947*10^{-8}$	1.0346

Table 4: Comparison of experimental and theoretical value of the polaronic concentration and polaronic conductivity.

Na vacancy concentration (%)	E_a **(Cal.) (eV)**	E_a **(Exp.) (eV)**	σ_{dc} **(Cal.)(S/cm)**	σ_{dc} **(Exp.) (S/cm)**
1.75	0.305	0.324	1.513×10^{-6}	1.63×10^{-6}
6	0.280	0.290	3.64×10^{-6}	3.05×10^{-6}
9.5	0.247	0.263	6.16×10^{-6}	4.02×10^{-6}
14.2	0.204	0.22	1.23×10^{-6}	8.32×10^{-5}

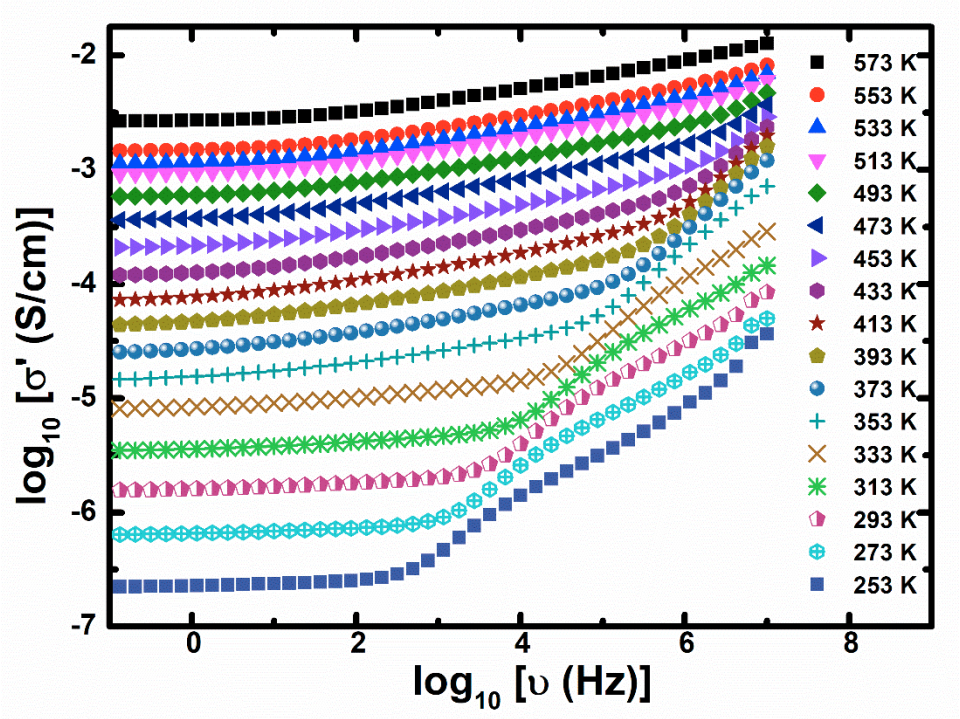

Figure 1: The real part of the frequency dependent ac conductivity for the bulk (80 nm crystallite size) sample measured by Broadband Impedance analyser varying the temperature from 253 K to 573 K. All the isotherms have been fitted with the Jonscher's relation to extract the dc conductivity.

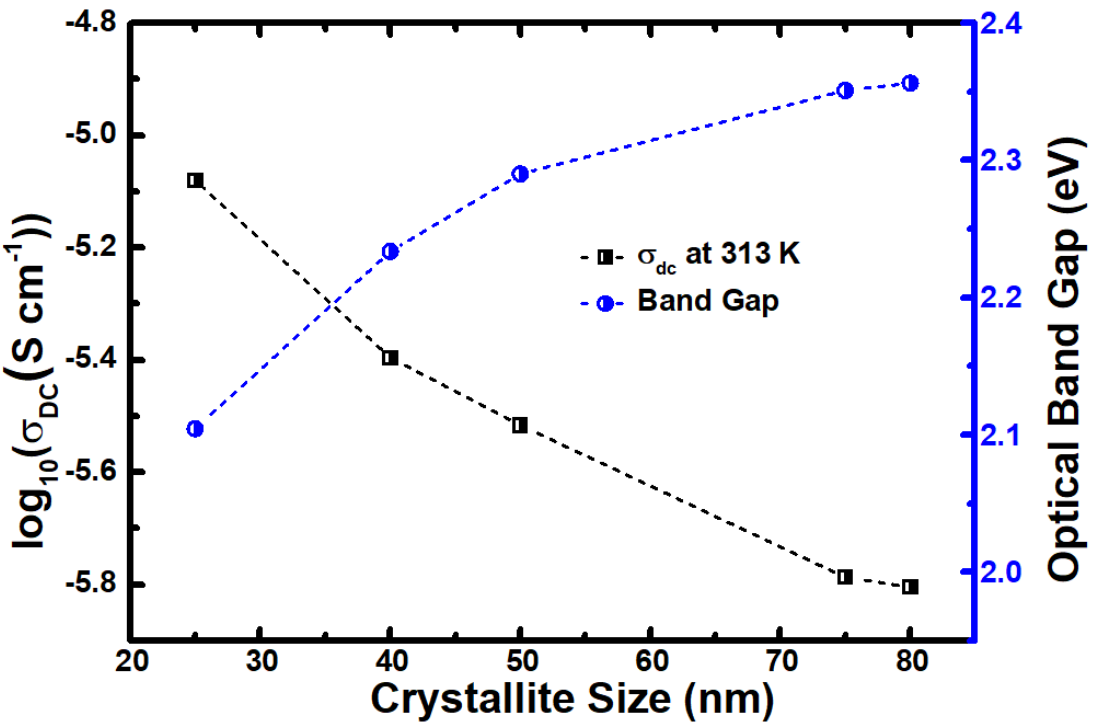

Figure 2: Variation of dc conductivity and optical band gap with the crystallite size. DC conductivity has been extracted by using the Jonscher's relation whereas the indirect optical band gap has been estimated by Tauc plot of the absorption spectra recorded by UV visible spectroscopy.

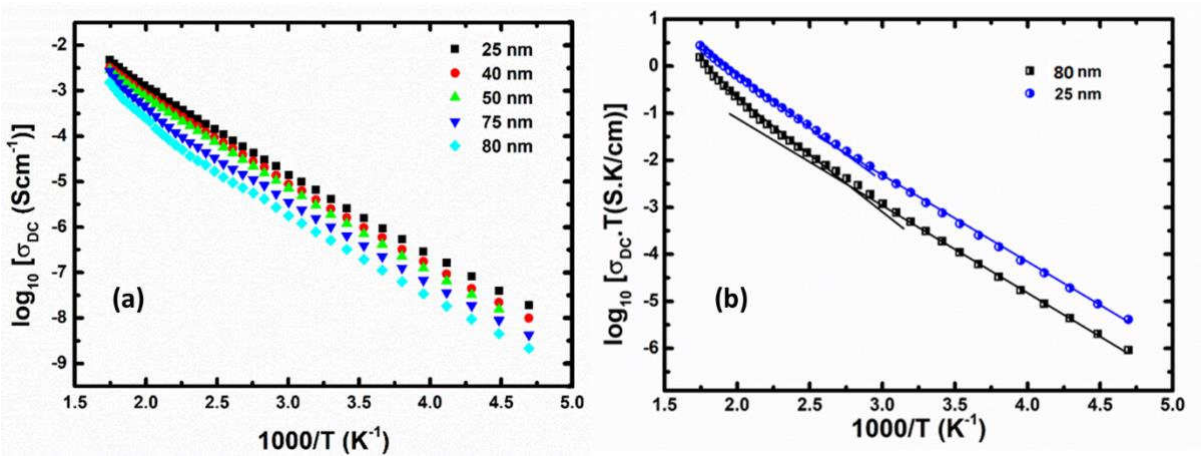

Figure 3: (a) The Arrhenius plot showing the variation of the DC conductivity over the temperature for the various crystallite sizes (b) Mott fitted Arrhenius plot for the bulk 80 nm and the lowest 25 nm crystallite sizes.

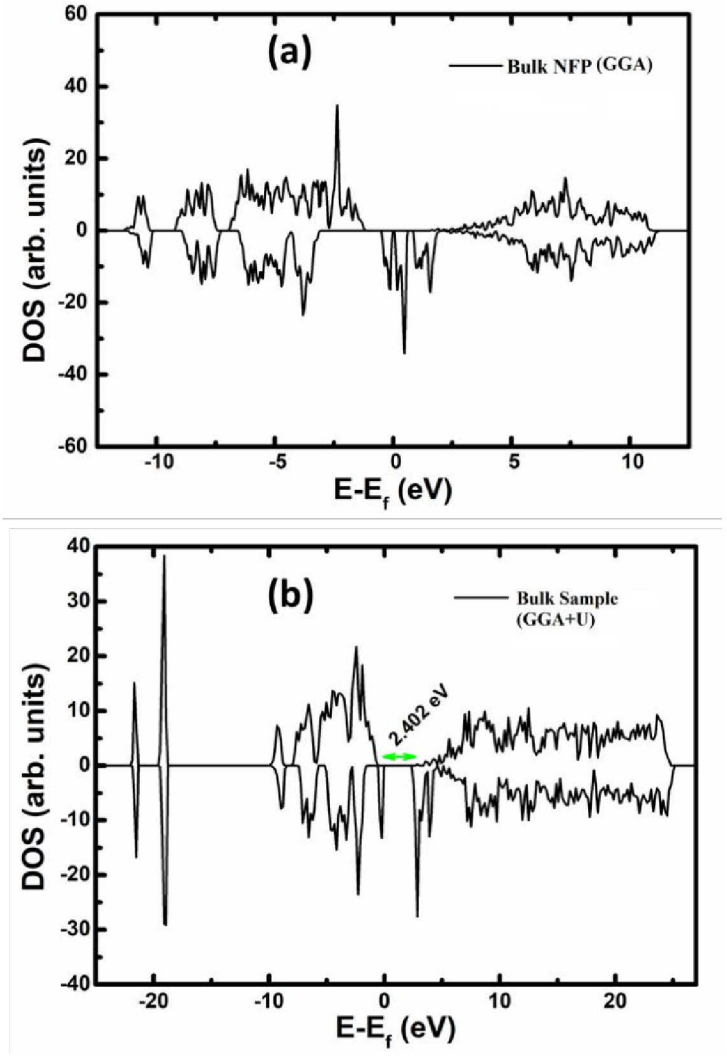

Figure 4: Calculated density of states for pristine bulk m-NFP with (a) PBE and (b) PBE+U (U=5.0 eV). Fermi level in both cases has been pinned to zero.

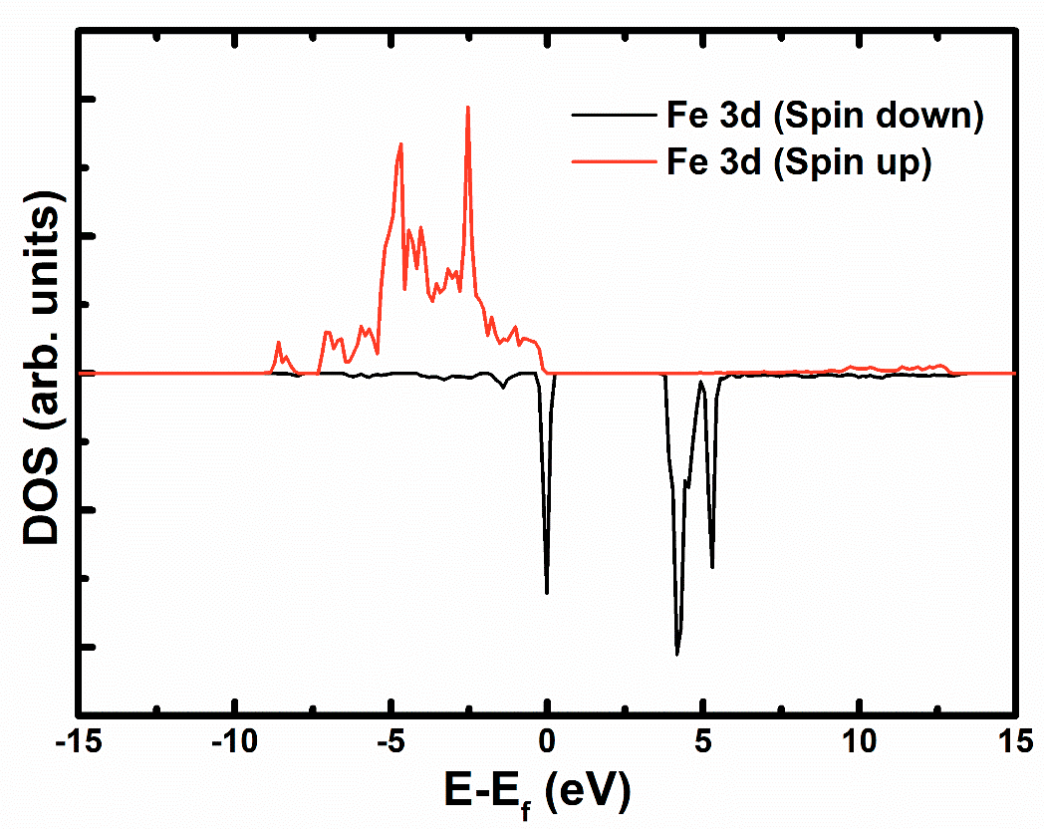

Figure 5: Spin polarized 3d_{Fe} band contribution to the total density of states in pristine bulk m-NFP.

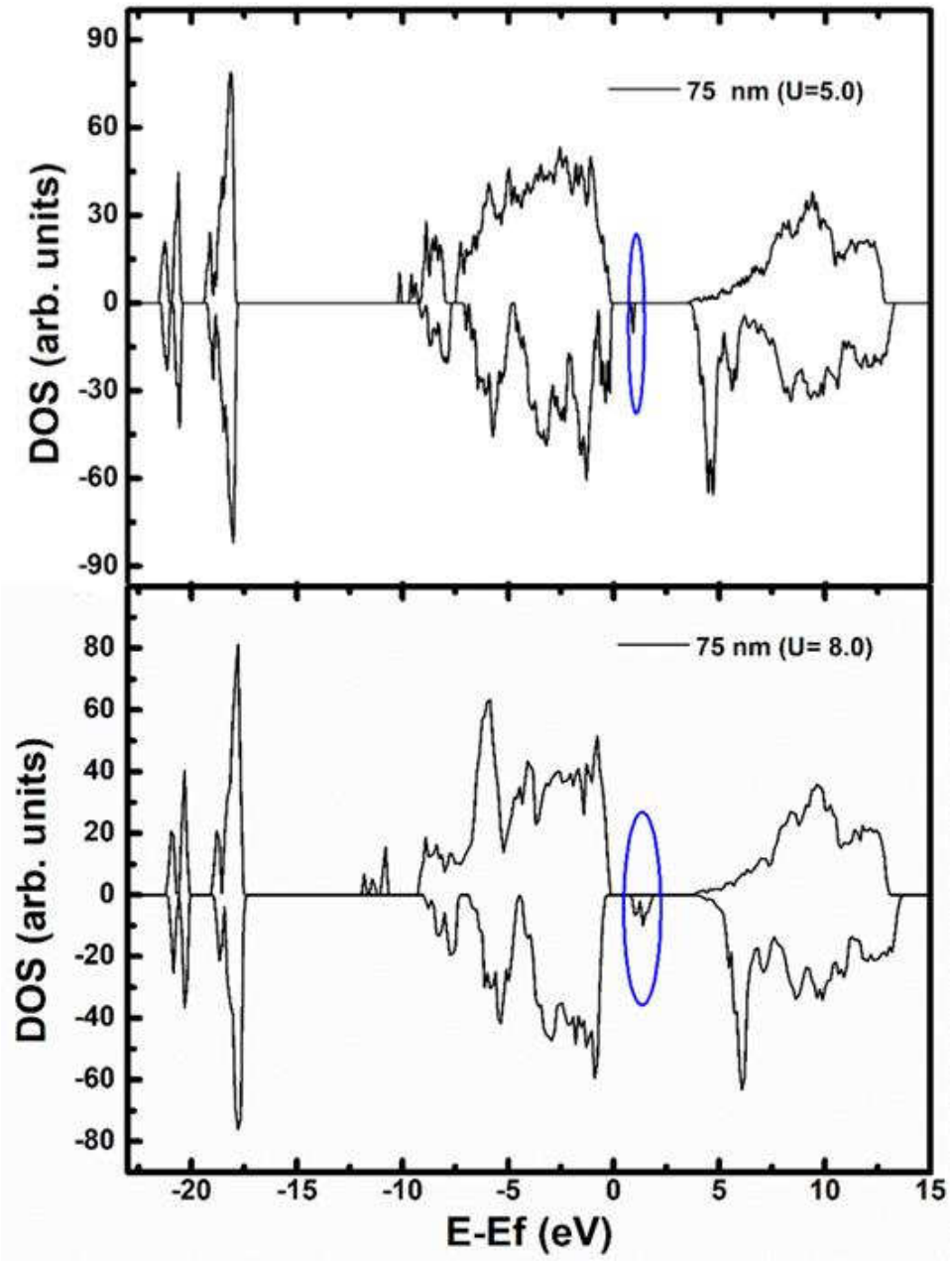

Figure 6: Density of states in bulk m-NFP with a trapped hole-polaron for the crystallite size of 75 nm calculated by using DFT-PBE with two different values of U.

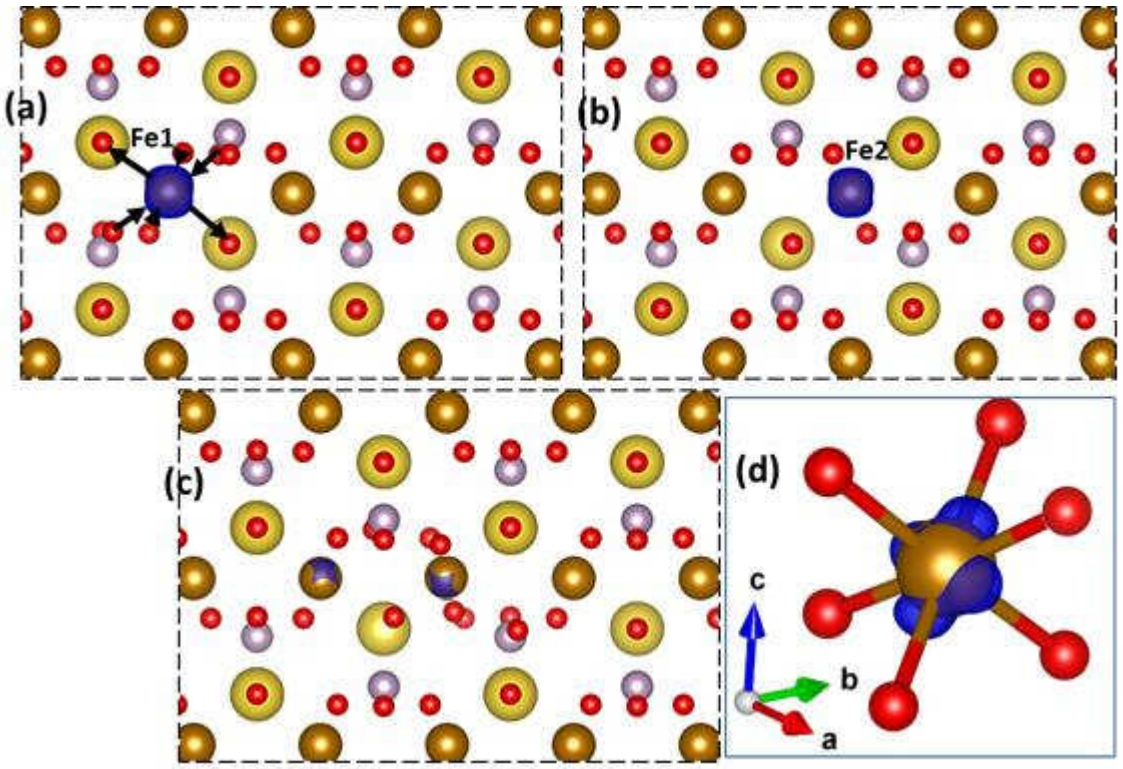

Figure 7: Spin density plots for (a) initial structure with hole-polaron centred at Fe1 site, (b) the final structure with hole-polaron centred at Fe2 site, and (c) transition state with hole-polaron centred at Fe1 and Fe2. (d) Zoomed view of isosurface of a hole in the initial state. Na, Fe, P, and O ions are in yellow, brown, light purple, and red, respectively.

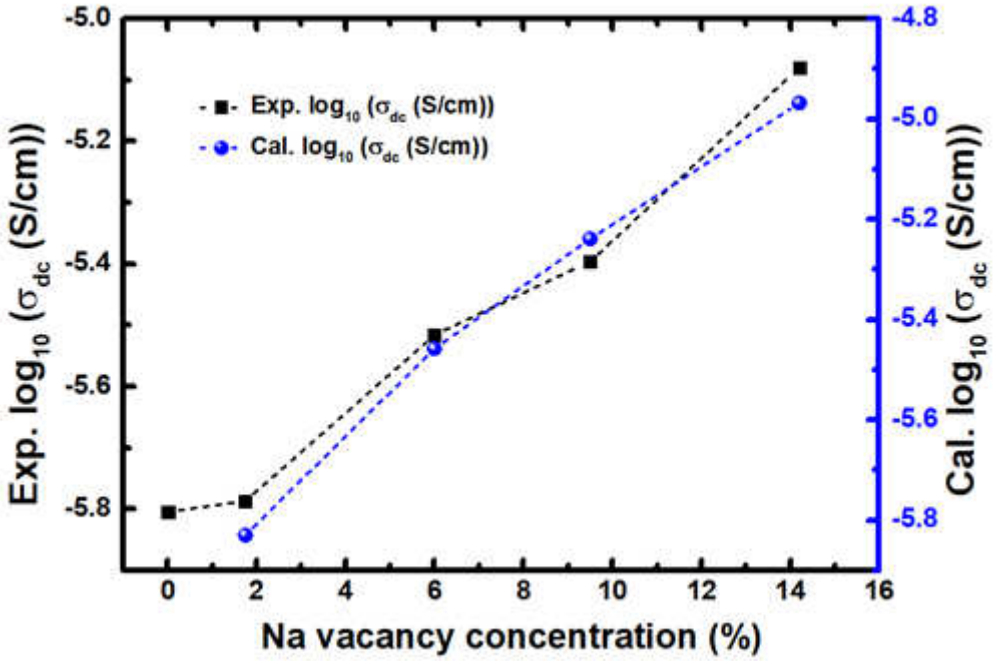

Figure 8: Experimental and theoretical polaronic conductivity as a function of Na_+ vacancy concentration.